Infrared Spectra and Density Functional Calculations for Three Pt−C_2H_2 Reaction Product Isomers: $PtCCH_2$, HPtCCH, and Pt−η^2-(C_2H_2)

Xuefeng Wang and Lester Andrews*

Department of Chemistry, P.O. Box 400319, University of Virginia, Charlottesville, Virginia 22904-4319

Received: February 20, 2004; In Final Form: March 22, 2004

Laser-ablated Pt atoms react with C_2H_2 upon co-condensation in excess argon and neon to form the vinylidene $PtCCH_2$, the insertion product HPtCCH, and the strong complex or metallacyclopropene Pt−η^2-(C_2H_2). These species are identified through $^{13}C_2H_2$, C_2D_2, and C_2HD isotopic substitutions and density functional theory isotopic frequency calculations. The global energy minimum $PtCCH_2$ is identified at 3022.4 cm^{-1} (C−H stretching), 1716.5 cm^{-1} (C−C stretching), and 707.9 cm^{-1} (CH_2 deformation) in an argon matrix. The C−C stretching modes for Pt−η^2-(C_2H_2) and HPtCCH are observed at 1653.7 and 2016.2 cm^{-1}, respectively. In addition, the insertion product HPtCCH is identified by a Pt−H stretching mode at 2350.8 cm^{-1} and a C−C stretching mode at 2010.4 cm^{-1} in the neon matrix. The most stable $PtCCH_2$ vinylidene isomer is the favored primary product. The strong complex Pd−η^2-(C_2H_2) rearranges by 1,2 hydrogen atom migration to form the vinylidene $PtCCH_2$ on 240−290 nm photolysis and on reaction during annealing solid neon to 10−12 K. These products are analogous to species formed from the adsorption and rearrangement of C_2H_2 on the Pt-(111) surface.

Introduction

The adsorption and associated rearrangement of C_2H_2 on platinum surfaces have been investigated extensively due to the importance of hydrocarbon hydrogenation and dehydrogenation.[1−6] Using vibrational spectroscopy Somorjai and co-workers have characterized C_2H_2 adsorption on the Pt(111) surface, which leads to the formation of η^2-μ_3-vinylidene at 125 K and upright bridge-bonded μ-vinylidene (Pt_2=C=CH_2) at 340 K.[5] Similar results were obtained by Avery on Pt(111) and King et al. on Pt(211).[4,6] Vinylidene surface intermediates are involved in hydrogen atom reactions in the hydrogenation of acetylene.[7]

The mechanism of the important acetylene−vinylidene rearrangement has been considered in a variety of environments, including gas phase[8−10] and transition metal complexes[11−14] in addition to the metal surface, as described for the platinum example.[1−6] Since the relative energies of the two isomers change markedly when a metal is involved, we wish to examine the effect of a single metal atom.

The matrix isolation technique has been used to investigate metal atom interactions with acetylene, and four bonding models, side-on M−η^2-(C_2H_2) (Cu, Ag, Au, Ni, Al, Li), vinyl form (Al, Au), inserted HMCCH (Be, B, Al, Fe), and vinylidene M=C=CH_2 (Ni, Au, Na) have been characterized by infrared and electron spin resonance spectroscopies.[15−25] However the bonding and reaction mechanism have not been studied for a single Pt atom with C_2H_2 since Pt is difficult to evaporate.

Our group has employed laser ablation to evaporate high-melting transition metals, which are co-condensed with reactive molecules and noble gas to trap transient intermediates and reaction products. Recently side-bonded palladium acetylene complexes, Pd−(η^2-C_2H_2)$_{1,2}$ have been identified by matrix infrared spectroscopy.[26] Analogous studies of transition metal reactions with dihydrogen have been investigated by this group, which established the simplest model to understand hydrogen activation and oxidative addition reactions.[27−31] It is significant that platinum inserts spontaneously into H_2 to form the PtH_2 dihydride.

In this paper we examine the reaction of laser-ablated Pt atoms with C_2H_2. The platinum vinylidene (Pt=C=CH_2), insertion product (HPtCCH), and strong platinum−acetylene complexes (Pt−η^2-(C_2H_2)$_{1,2}$) are all observed through matrix infrared spectra. The structures, vibrational frequencies, and infrared intensities are confirmed by isotopic substitution and density functional theory (DFT) frequency calculations. The thermally and photolytically induced rearrangements and reactions of Pt with C_2H_2 are discussed and compared to platinum surface chemistry.

Experimental and Theoretical Methods

Pulsed-laser ablation was employed to vaporize platinum atoms,[27,32,33] which reacted with C_2H_2 in excess argon or neon, and reaction products were co-deposited onto a 7 or 4 K CsI cryogenic window with excess argon or neon. The Nd:YAG laser fundamental (1064 nm, 10 Hz repetition rate with 10 ns pulse width) was focused onto a rotating platinum target, and a bright ablation plume was produced. Infrared spectra were recorded at 0.5 cm^{-1} resolution on a Nicolet 750 with 0.1 cm^{-1} accuracy using an MCTB detector. Isotopic substitution ($^{13}C_2H_2$, C_2D_2, and C_2HD) was used for band identification. Matrix samples were subjected to photolysis by UV−vis irradiation using a medium-pressure mercury arc lamp.

Density functional theory frequency calculations were done to reproduce the structures and frequencies of platinum−acetylene complexes and radicals using the Gaussian 98 program.[34] BPW91 and B3LYP density functionals[35,36] with 6-311++G(d,p) basis sets for C and H atoms[37] and the SDD pseudopotential for Pt atom were employed.[38] Geometries were fully optimized, and the vibrational frequencies were calculated analytically from second derivatives.

* To whom correspondence should be addressed. E-mail: lsa@virginia.edu.

10.1021/jp049218o CCC: $27.50
Published on Web 05/04/2004

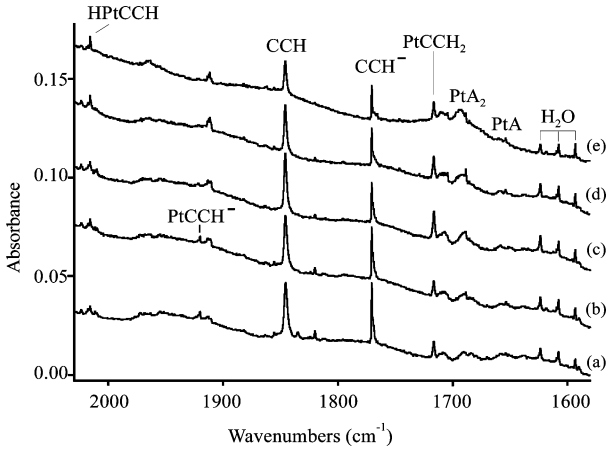

Figure 1. Infrared spectra in the 1580−2030 cm^{-1} region for laser-ablated Pt co-deposited with 0.5% C_2H_2 in argon at 7 K: (a) spectrum after sample deposited for 60 min, (b) after annealing to 25 K, (c) after $\lambda > 240$ nm photolysis, (d) after annealing to 30 K, and (e) after annealing to 35 K.

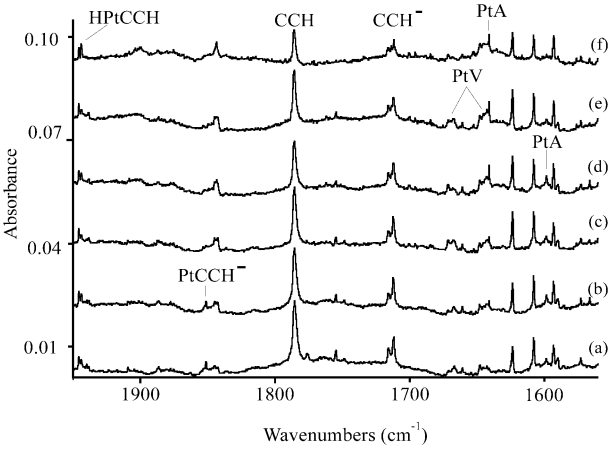

Figure 2. Infrared spectra in the 1560−1950 cm^{-1} region for laser-ablated Pt co-deposited with 0.5% $^{13}C_2H_2$ in argon at 7 K: (a) spectrum after sample deposited for 60 min, (b) after annealing to 25 K, (c) after $\lambda > 290$ nm photolysis, (d) after annealing to 30 K, (e) after $\lambda > 290$ nm photolysis, and (f) after annealing to 35 K.

Results

Infrared Spectra. Figures 1−3 show the infrared spectra of laser-ablated Pt atom reactions with C_2H_2 in excess argon at 7 K. The measured absorptions of various reaction products are listed in Table 1. Absorptions common to metal−acetylene experiments include acetylene, weak acetylene aggregates, and the intermediates CCH (1846.1, 2103.5 cm^{-1}), CCH^+ (1820.2 cm^{-1}), CCH^- (1770.5 cm^{-1}), C_4H (2060.4 cm^{-1}), C_4 (1543.3 cm^{-1}), C_4H_2 (627.7 cm^{-1}), and weak PtNN (2168.5 cm^{-1}), which have been reported previously.[39−43] In addition PtH (2280.4 cm^{-1}) and PtH_2 (2348.9 cm^{-1}) are observed as reaction products.[27] These experiments have minimal oxygen impurity since no PtO_2 is detected at 953.3 cm^{-1}.[32] The new product bands unique to Pt are grouped as A, B, C, and D according to their behavior on sample annealing, wavelength-dependent photolysis, and isotopic substitution. Group A bands at 3022.4, 1716.5, and 707.9 cm^{-1} appear on deposition, decrease by 10% on annealing to 25 K, but double their intensities on broadband photolysis and decrease again on further annealing to 30 and 35 K. With C_2D_2 three bands shift to 2218.9, 1662.6, and 566.5 cm^{-1}. Group B consists of 2016.2 and 577.5 cm^{-1} bands, which are unchanged on photolysis. Group C absorbs at 1653.7, 882.8, and 666.2 cm^{-1}, which increase on annealing but decrease on photolysis. These bands show larger isotopic shifts with both ^{13}C and deuterium substitutions than group A bands, suggesting a different bonding form. One broad band with sharp shoulder at 1688.6 cm^{-1} increases on annealing and forms the D group.

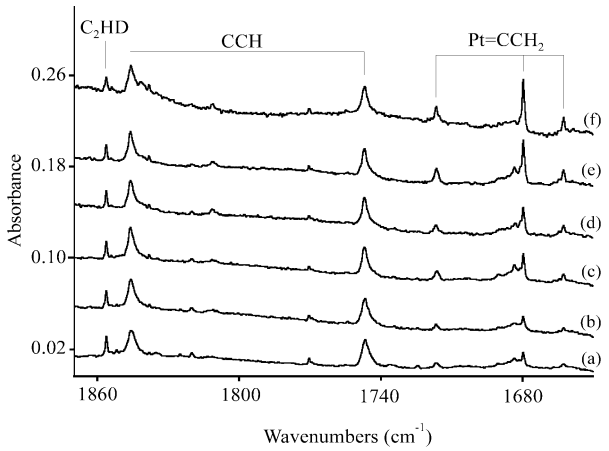

Figure 3. Infrared spectra in the 1650−1870 cm^{-1} region for laser-ablated Pt co-deposited with mixed 0.15% C_2H_2 + 0.25% C_2HD + 0.10% C_2D_2 in argon at 7 K: (a) spectrum after sample deposited for 60 min, (b) after annealing to 25 K, (c) after $\lambda > 240$ nm photolysis, (d) after annealing to 30 K, and (e) after annealing to 35 K.

TABLE 1: Infrared Absorptions (cm^{-1}) Observed for Pt + C_2H_2 Reaction Products in Solid Argon at 7 K

C_2H_2	$^{13}C_2H_2$	C_2D_2	assignment[a]
3104.5	3095.0	2311.5	$C_2H_2^+$
3022.8	3013.4	2218.9	$PtCCH_2$ (A)
2348.9	2348.9	1683.3	PtH_2
2280.4	2280.4	1634.0	PtH
2142.0	2080.0	2112.4	CH_2CO
2084.0	2005.7	2056.5	C_xH_y
2060.4	1981.5	2049.4	C_4H
2016.2	1944.3	1890.9	HPtCCH (B)
1920.5	1851.2	1825.2	$PtCCH^-$
1912.0	1843.4	1811.4	$[PtCCH^-]X$
1845.8	1785.5	1746.5	CCH
1820.2	1754.9	1724.4	CCH^+
1770.5	1711.8	1676.7	CCH^-
1716.5	1667.4, 1648.1	1662.6	$PtCCH_2$ (A)
1688.6	1640.9	1574.2	$Pt(C_2H_2)_2$ (D)
1653.7	1598.5	1550.9	$Pt(C_2H_2)$ (C)
1618.3	1566.2	1534.3	$[Pt(C_2H_2)]X$
882.8	873.4	731.1	$Pt(C_2H_2)$ (C)
707.9	701.1	566.6	$PtCCH_2$ (A)
666.2	663.2	499.9	$Pt(C_2H_2)$ (C)
627.7	622.4	495.6	C_4H_2
599.7	592.1	482.2	?
577.5	571.0	475.8	HPtCCH (B)
575.0	569.1	474.5	HPtCCH site

[a] Band group designation given in parentheses.

Complementary spectra from neon matrix experiments are illustrated in Figures 4 and 5, and the bands are listed in Table 2. The slower condensation rate of neon allows more precursor aggregation as attested by Pt_2 electronic bands[44] at 1942, 2143, and 2343 cm^{-1} and $(C_2H_2)_n$ clusters at 1970.4, 1967.5 cm^{-1} just below the symmetric C−C stretching fundamental of C_2H_2 at 1973.8 cm^{-1} in the gas phase.[45] Group A bands are shifted to 3033.9, 1712.6, and 720.8 cm^{-1}. Matrix shifts from C_2H_2 and CO_2 make possible the observation of two new group B bands at 3317.5 and 2350.8 cm^{-1} plus counterparts at 2010.4 and 571.5 cm^{-1}. Group C bands appeared at 1658.4, 878.6, and 665.9 cm^{-1} and gave way to the D band at 1693.5 cm^{-1} on annealing.

Calculations. The structures and frequencies of expected platinum acetylene complexes, isomers and radicals are calcu-

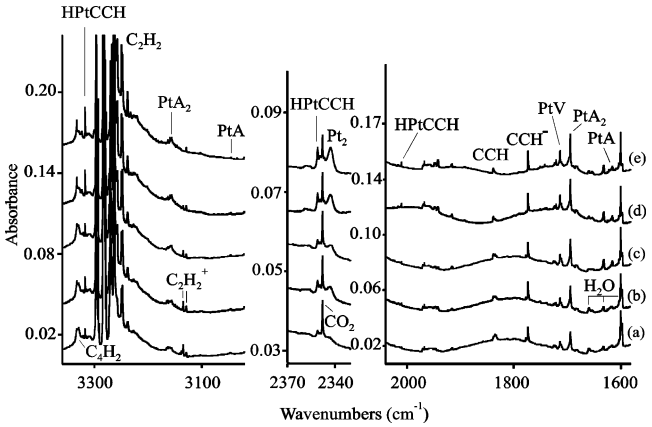

Figure 4. Infrared spectra in selected regions for laser-ablated Pt co-deposited with 0.3% C_2H_2 in neon at 4 K: (a) spectrum after sample deposited for 60 min, (b) after annealing to 10 K, (c) after $\lambda > 240$ nm photolysis, (d) after annealing to 12 K, and (e) after annealing to 14 K.

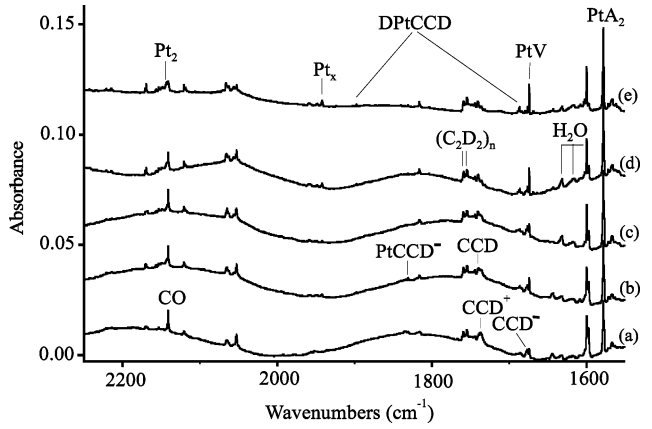

Figure 5. Infrared spectra in selected regions for laser-ablated Pt co-deposited with 0.2% C_2D_2 in neon at 4 K: (a) spectrum after sample deposited for 60 min, (b) after annealing to 10 K, (c) after $\lambda > 240$ nm photolysis, (d) after annealing to 12 K, and (e) after annealing to 14 K.

lated and the results are listed in Tables 3−7. Three isomers are located on the Pt−C_2H_2 singlet potential energy surface, namely, Pt−vinylidene, Pt−η^2-C_2H_2, and the inserted HPtCCH molecule. Platinum vinylidene in the $^1A_1$ ground state is the global energy minimum structure with both BPW91 and B3LYP functional calculations. The Pt atom bonds to the terminal C atom in vinylidene (shown in Figure 6), which is an important reaction intermediate. The calculated Pt−C double bond length is 1.759 Å (BPW91) and 1.766 Å (B3LYP), which is much shorter than the Pt−C bond length in Pt−C_2H_2 complexes. The C−C distance, 1.313 Å (BPW91) and 1.304 Å (B3LYP), shows double CC bond character. The side-bound Pt−C_2H_2 complex, Pt−η^2-C_2H_2, lies 3.6 kcal/mol higher in energy than ground-state Pt═CCH_2, and the CC bond is calculated to be 1.288 Å (BPW91) and 1.271 Å (B3LYP), respectively. This is 0.02 Å longer than the CC bond in the Pd−η^2-C_2H_2 complex,[26] indicating a stronger interaction between C_2H_2 and Pt atom. It is interesting to note for free C_2H_2 and vinylidene (CCH_2) theoretical and experimental studies found that CCH_2 is 44−47 kcal/mol higher in energy than C_2H_2.[8−10] Here the relative energies are reversed when coordinated to a platinum atom. The third isomer, HPtCCH, is 10.6 kcal/mol higher in energy than ground-state Pt═CCH_2. For this molecule the Pt atom inserts into a C−H bond in C_2H_2 and the triple CC bond remains in contrast to the double bond in Pt═CCH_2. The calculated

TABLE 2: Infrared Absorptions (cm^{-1}) Observed for Pt + C_2H_2 Reaction Products in Solid Neon at 4 K

C_2H_2	$^{13}C_2H_2$	C_2D_2	assignment[a]
3332.9	3315.4	2597.6	C_4H_2
3317.5	3301.4	2577.8	HPtCCH (B)
3159.2	3149.5	2351.4	$Pt(C_2H_2)_2$
3157.7	3147.8	2350.1	$Pt(C_2H_2)_2$
3156.0	3145.9	2348.8	$Pt(C_2H_2)_2$
3134.7	3125.8	2327.2	$C_2H_2^+$
3128.4	3119.3	2339.1	$Pt(C_2H_2)$
3033.9		2221.1	$PtCCH_2$ (A)
2355.2	2355.2	1688.2	PtH_2
2350.8	2350.8	1685.9	HPtCCH
2347.7	2347.7	2347.7	CO_2
2343	2343	2343	Pt_2
2143	2143	2143	Pt_2
2063.7	1984.7	2052.5	C_4H
2010.4	1938.6	1897.2	HPtCCH (B)
1970.4		1759.0	$(C_2H_2)_n$
1967.5	1904.3	1754.2	$(C_2H_2)_n$
1942	1942	1942	Pt_x
1924.4		1830.2	$PtCCH^-$
1915.9	1847.2	1815.4	$[PtCCH^-]X$
1838.1	1778.7	1739.7	CCH
1835.2	1775.6	1737.2	CCH
1832.2	1767.6	1735.1	CCH^+
1773.0	1717.0	1675.7	CCH^-
1722.6		1677.9	$PtCCH_2$ site
1720.3			$PtCCH_2$ site
1712.6	1671.0, 1645.8	1673.4	$PtCCH_2$ (A)
1693.5	1645.0	1577.6	$Pt(C_2H_2)_2$ (D)
1658.4	1599.0	1571.2	$Pt(C_2H_2)$ (C)
1652.0		1566.5	$Pt(C_2H_2)$ site
1623.9	1573.5	1530.2	$[Pt(C_2H_2)]X$
1620.8	1569.6	1527.8	$[Pt(C_2H_2)]X$
878.6	869.5	724.4	$Pt(C_2H_2)$ (C)
872.6	863.6	717.7	$Pt(C_2H_2)$ site
720.8	717.6		$PtCCH_2$ (A)
665.9	663.1	500.5	$Pt(C_2H_2)$ (C)
664.2	661.3	498.3	$Pt(C_2H_2)$ site
630.8	625.8	497.3	C_4H_2
596.7	592.3	454.8	
571.5	567.7	444.8	HPtCCH (B)
514.6	512.0	-	HPtCCH (B)

[a] Band group designation given in parentheses.

H−Pt−C right angle is 90.3° (BPW91) and 90.5° (B3LYP), respectively, slightly larger than the H−Pt−H angle calculated at the same level. Figure 7 shows an energy profile for the Pt−C_2H_2 isomers.

When two Pt atoms interact with C_2H_2, two isomers, Pt_2−CCH_2 and Pt_2−η^2-C_2H_2, are found with total energies very close to those of the present calculations. The Pt_2−CCH_2 form is the global energy minimum, and Pt_2−η^2-C_2H_2 lies 0.6 kcal/mol higher at the BPW91 level. Note the C−C bond is lengthened to 1.337 Å in Pt_2−η^2-C_2H_2, inferring the C−C triple bond is reduced to a double bond.

Finally the PtCCH and $PtCCH^-$ species are calculated to reproduce the observed spectra. At the BPW91 level the C−C bonds are predicted to be 1.223 Å for PtCCH and 1.241 Å for $PtCCH^-$, which are essentially triple C−C bonds.

Discussion

New product absorptions will be assigned on the basis of frequency shifts with $^{13}C_2H_2$ and C_2D_2 substitution, isotopic distributions with mixed C_2H_2 + C_2HD + C_2D_2, and DFT frequency calculations.

Pt═C═CH_2. Group A bands double intensity on broad-band photolysis and are assigned to Pt═C═CH_2. The diagnostic band for this identification is the C═C double bond stretching mode

TABLE 3: Geometries and Frequencies Calculated at the BPW91/6-311++G(d,p)/ SDD Level of Theory for Platinum Acetylene Complexes

Molecule	state	rel energy, kcal/mol	geometries (length, Å; angle, deg)	frequencies, cm^{-1} (intensities, km/mol)
C_2H_2	$^1\Sigma_g^+$	-	CC, 1.209; CH, 1.070	3463.2 (0,σ_g), 3363.9 (84, σ_u), 2005.4 (0, σ_g), 742.0 (109,π_u), 584.4 (0,π_g)
PtCCH ($C_{\infty v}$)	$^2\Sigma$	0.0a	CC, 1.223; CH, 1.069; PtC, 1.876	3411.1 (σ,680), 2037.1 (σ,28), 597.4 (π,144), 594.8 (π,141×2), 530.3 (σ,0), 269.3 (π,13×2)
$PtCCH^-$ ($C_{\infty n}$)	$^1\Sigma$	-65.7	CC, 1.241; CH, 1,068; PtC, 1.841	3407.5 (σ,50), 1942.5 (σ,388), 557.1 (σ,0), 355.7 (π,108×2), 290.5 (π,22×2)
$PtCCH_2$ (C_{2v})	$^1A_1$	0.0	PtC, 1.759; CC, 1.313; CH, 1.092; PtCC, 180.0; HCH, 119.2	3160.1 (b_2,8), 3075.9 (a_1,30), 1720.9 (a_1,231), 1281.8 (a_1,3), 803.5 (b_2,6), 654.8 (b_1,92), 612.3 (a_1,2), 315.9 (b_1,22), 284.2 (b_2,15)
Pt−η^2-C_2H_2 (C_{2v})	$^1A_1$	3.6	PdC, 1.993; CC, 1.288; CH, 1.081; CPdC, 37.7; CCH, 153.2	3269.4 (a_1,3), 3213.9 (b_2,21), 1651.8 (a_1,10), 858.0 (b_2,76), 836.6 (a_1,1), 651.9 (b_1,71), 591.6 (a_2,0), 549.2 (a_1,7), 493.8 (b_2,2)
HPtCCH (C_s)	^1A	10.6	PtH, 1.526; PtC, 1.865; CC, 1.225; CH, 1.069; HPtC, 90.4; PtCC, 180.	3410.3 (74), 2421.1 (17), 2023.9 (12), 626.1 (32), 580.5 (51), 546.3 1), 530.5(73), 277.1 (10), 243.8 (10)
Pt−η^2-C_2H_2 (C_{2v})	$^3B_1$	40.5	PdC, 2.027; CC, 1.289; CH, 1.082; CPdC, 37.1; CCH, 153.9	3275.2 (a_1,11), 3217.2 (b_2,24), 1639.2 (a_1,1), 780.2 (b_2,26), 774.3 (a_1,11), 712.7 (a_2,0), 687.2 (b_1,55), 449.3 (a_1,3), 50.9 (b_2,19)
Pt−η^2-$(C_2H_2)_2$ (D_{2d})	$^1A_1$	0.0	PtC, 2.037; CC, 1.279; CH, 1.081; CPdC, 36.6; CCH, 153.0	3273.6 (b_2,8), 3273.5 (a_1,0), 3217.8 (e,13×2), 1708.0 (b_2,94), 1680.7 (a_1,0), 841.5(e,45×2), 826.6 (b_2,13), 802.7 (a_1,0), 730.1(b_1,0), 725.3 (e,38×2), 714.7 (a_2,0), 571.0 (e,3×2), 500.0 (b_2,3), 498.5 (a_1,0), 257.3 (b_1,0), 136.9 (e,7×2)
Pt_2−CCH_2 (C_{2v})	$^1A_1$	0.0	PtC, 1.921; CC, 1.334; CH, 1.092; PtPt, 2.558; PtCPt, 83.5; HCH, 118.1	3147.8 (b_2,0), 3063.9 (a_1,2), 1595.6 (a_1,129), 1322.0 (a_1,0), 934.4 (b_2,2), 715.8 (b_1,67), 556.7 (b_2,8), 512.2 (a_1,1), 347.4 (a_2,0), 338.2 (b_1,18), 205.1 (b_2,0), 171.8 (a_1,0)
parallel Pt_2−η^2-C_2H_2 (C_{2v})	$^1A_1$	0.6	PtC, 1.944; CC, 1.337; CH, 1.095; PtPt, 2.557; PtCC, 108.3; CCH, 131.4	3094.6 (a_1,0), 3066.4 (b_2,0), 1491.8 (a_1,43), 1090.5 (b_2,17), 953.6 (a_1,13), 651.7 (b_2,8), 630.0 (a_1,2), 629.0 (a_2,0), 585.9 (b_1,72), 321.8 (b_2,0), 247.4 (a_2,0), 171.5 (a_1,0)

[a] $\langle S^2 \rangle$ value is 0.7514 before annihilation.

at 1716.5 cm^{-1}, which shows a much smaller deuterium shift than this mode in Pt−η^2-(C_2H_2) and HPtCCH. The 1716.5 cm^{-1} band shifts to 1662.6 cm^{-1} with C_2D_2, giving a 1.0324 H/D isotopic ratio frequency and showing coupling with C−H(D) motion. Using a mixed $C_2H_2 + C_2HD + C_2D_2$ sample, a triplet distribution is observed at 1716.5, 1679.8, and 1662.6 cm^{-1} (Figure 2), indicating that two equivalent H atoms are involved in this molecule. With $^{13}C_2H_2$ this band splits into absorptions at 1671.5 and 1648.1 cm^{-1}; based on DFT calculations, the in-plane CH_2 bending overtone for Pt═C═CH_2 with ^{13}C substitution appears in this region and is responsible for a Fermi resonance splitting (Figure 3). The 3022.4 cm^{-1} absorption shifts to 3013.4 cm^{-1} with ^{13}C and to 2218.9 cm^{-1} with D (H/D = 1.362), and one new band is observed at 2259.7 cm^{-1} with the $C_2H_2 + C_2HD$ and C_2D_2 sample. The 3022.4 cm^{-1} band is appropriate for C−H stretching in Pt═C═CH_2, which is slightly lower than the 3033 cm^{-1} absorption of μ-vinylidene on Pt(111) but higher than absorptions of surface-adsorbed species, η^2-μ_3-vinylidene, ethylidene, and di-σ-bonded ethylene.[4−6] A band at 707.9 cm^{-1} tracks with the 3022.4 and 1716.5 cm^{-1} bands and shifts to 701.1 upon ^{13}C substitution. This mode is the deformation vibration for the CCH_2 moiety. The deuterium counterpart shifted to 566.6 cm^{-1}, and a sharp triplet is observed with $C_2H_2 + C_2HD + C_2D_2$ at 707.9, 639.8, and 566.6 cm^{-1}.

Neon matrix counterparts were observed at 3033.9, 1712.6, and 720.8 cm^{-1} for $PtCCH_2$. This represents 11.5 cm^{-1} blue, 3.9 cm^{-1} red, and 12.9 cm^{-1} blue shifts. Neon matrix bands for $PtCCD_2$ at 2221.1 and 1673.4 cm^{-1} exhibit 2.2 and 10.8 cm^{-1} blue shifts. Such small shifts are typical,[46] but it appears that matrix interaction affects the a_1 CH_2, C═C mode mixing. In contrast to argon, the $PtCCH_2$ bands increase slightly on annealing in the softer neon matrix (+25% for 12 K annealing).

DFT frequency calculations with BPW91 and B3LYP functionals for $PtCCH_2$ are in excellent agreement with experimental values. At the BPW91 level the predicted a_1 C−H and C−C stretching modes are at 3075.9 and 1720.9 cm^{-1}, respectively, only overestimated by 53.1 and 4.4 cm^{-1}, respectively, but at the same level the out-of-plane deformation mode is underestimated by 53.1 cm^{-1}. The B3LYP calculations give slightly higher frequencies for these three modes, but they still match the experiment very well. In particular the out-of-plane mode is described more accurately by B3LYP. Higher level calculations are needed for this important molecule.

Table 5 compares calculated and observed isotopic frequencies for $PtCCH_2$. The stronger observed a_1 CH_2 stretching mode has calculated (observed) 6.2 (9.0) cm^{-1} and 839.5 (805.5) cm^{-1} ^{13}C and D shifts, respectively. The C−D stretching mode for PtCCHD is predicted 46.5 cm^{-1} and observed 40.8 cm^{-1} above the a_1 mode for $PtCCD_2$. The C═C stretching mode has 66.7 (68.4) cm^{-1} and 35.9 (53.9) cm^{-1} ^{13}C and D shifts, respectively. The out-of-plane deformation mode for PtCCHD is predicted 3.0 above the median for $PtCCH_2$ and $PtCCD_2$, and the observed frequency is 2.6 cm^{-1} above the median observed value. The ^{13}C shifts are 7.2 (6.8) cm^{-1}. Finally, the calculated relative infrared intensities are in good agreement with the observed band absorbances except that the out-of-plane deformation is double the intensity predicted. This discrepancy may arise from anharmonicity in the observed mode.

HPtCCH. Group B bands at 2016.2 and 577.5 cm^{-1} show no change on photolysis but increase 25% on annealing to 30

TABLE 4: Geometries and Frequencies Calculated at the B3LYP/6-311++G(d,p)/ SDD Level of Theory for Platinum Acetylene Complexes

molecule	state	rel energy, kcal/mol	geometries (length, Å; angle, deg)	frequencies, cm^{-1} (intensities, km/mol)
C_2H_2	$^1\Sigma_g^+$		CC, 1.209; CH, 1.070	3463.2 (0,σ_g), 3363.9 (84, σ_u), 2005.4 (0,σ_g), 742.0 (109,π_u), 584.4 (0,π_g)
PtCCH ($C_{\infty v}$)	$^2\Sigma$	0.0[a]	CC, 1.212; CH, 1.063; PtC, 1.896	3470.1 (101), 2099.9 (38), 619.7 (55), 605.9 (36), 516.1 (1), 269.0 (20), 243.7 (20)
$PtCCH^-$ (C_{2v})	$^1\Sigma$	−61.9	CC, 1.228; CH, 1.061; PtC, 1.858	3471.3 (σ,46), 2004.3 (σ,374), 537.8 (σ,1), 442.6 (π,114×2), 327.3 (π,11×2)
Pt−CCH_2 (C_{2v})	$^1A_1$	0.0	PtC, 1.766; CC, 1.304; CH, 1.086; PtCC, 180.0; HCH, 119.3	3211.8 (b_2,7), 3127.6 (a_1,30), 1751.3 (a_1,252), 1326.2 (a_1,1), 828.3 (b_2,9), 725.6 (b_1,87), 603.6 (a_1,3), 315.6 (b_1,25), 290.4 (b_2,16)
Pt−η^2-C_2H_2 (C_{2v})	$^1A_1$	2.7	PtC, 2.009; CC, 1.271; CH, 1.074; CPtC, 36.9; CCH, 153.5	3341.4 (a_1,4), 3282.7 (b_2,28), 1716.9 (a_1,15), 877.7 (b_2,82), 848.4 (a_1,3), 689.5 (b_1,74), 663.5 (a_2,0), 525.9 (a_1,7), 488.7 (b_2,3)
HPtCCH (Cs)	^1A	9.0	PtH, 1.522; PtC, 1.880; CC, 1.213; CH, 1.063; HPtC, 90.5; PtCC, 180.	3469.4 (77), 2436.6 (13), 2093.2 (8), 652.7 (62), 636.5 (22), 607.2 (67), 536.6 (2), 287.9 (16), 252.0 (14)
Pt−η^2-$(C_2H_2)_2$ (D_{2d})	$^1A_1$	0.0	PtC, 2.049; CC, 1.264; CH, 1.073; CPdC, 35.92; CCH, 153.8	3347.1 (b_2,16), 3346.8 (a_1,0), 3287.5 (e,20×2), 1767.9 (b_2,112), 1742.4 (a_1,0), 867.0 (e,45×2), 833.4 (b_2,22), 814.6 (a_1,0), 765.5 (b_1,0), 753.5 (a_2,0), 750.2 (e,42×2), 565.9 (e,2×2), 485.3 (b_2,8), 476.2 (a_1,0), 261.2 (b_1,0), 133.8 (e,6×2)
parallel Pt_2–C_2H_2 (C_{2v})	$^1A_1$	0.0	PtC, 1.824; CC, 1.455; CH, 1.097; PtPt, 3.636; PtCC, 126.7; CCH, 115.5	3047.6 (a_1,9), 3025.1 (b_2,2), 1316.4 (a_1,12), 1188.1 (b_2,18), 1098.6 (a_1,23), 1071.5 (b_2,0), 801.5 (b_1,1), 633.9 (a_1,0), 601.7 (b_1,68), 392.7 (b_2,2), 234.9 (a_2,0), 52.3 (a_1,0)
Pt_2−CCH_2 (C_{2v})	$^1A_1$	14.9	PtC, 1.886; CC, 1.403; CH, 1.087; PtPt, 3.557; PtCPt, 125.8; HCH, 117.4	3209.3 (b_2,2), 3108.7 (a_1,0), 1476.2 (a_1,0), 1237.6 (a_1,77), 1075.2 (b_2,3), 997.6 (b_1,4), 764.1 (b_2,0), 420.4 (a_2,1), 401.3 (a_1,10), 237.9 (b_2,1), 96.6 (a_1,0), 78.7 (b_1,4)

[a] $\langle S^2 \rangle$ value is 0.7511 before annihilation.

TABLE 5: Comparison of Calculated (B3LYP) and Observed (Argon Matrix) Isotopic Frequencies (cm^{-1}) for $PtCCH_2$

$PtCCH_2$		$Pt^{13}C^{13}CH_2$		PtCCHD		$PtCCD_2$	
calc	obs	calc	obs	calc	obs	calc	obs
3211.8 (b_2, 7)[a]	n.o.[b]	3198.9	n.o.	3172.3	n.o.	2388.1	n.o.
3127.6 (a_1, 30)	3022.4 (0.0018)[c]	3121.4	3013.4	2334.6	2259.7	2288.1	2218.9
1751.3 (a_1, 252)	1716.5 (0.014)	1684.6	1648.1	1734.1	1679.8	1715.4	1662.6
725.6 (b_1, 87)	707.9 (0.0087)	718.4	701.1	655.1	639.8	578.7	566.6

[a] Mode symmetry, intensity (km/mol). [b] Not observed. [c] Intensity, absorbance units, after full-arc photolysis.

TABLE 6: Comparison of Calculated (BPW91) and Observed (Neon Matrix) Isotopic Frequencies (cm^{-1}) for HPtCCH

HPtCCH		$HPt^{13}C^{13}CH$		DPtCCD	
calc	obs	calc	obs	calc	obs
3410.2 (74)[a]	3317.5 (0.018)[b]	3392.9	3301.4	2626.3	2577.8
2421.5 (17)	2350.8 (0.0030)	2421.4	2350.8	1905.3	1897.2
2023.7 (12)	2010.4 (0.0026	1950.5	1938.6	1715.7	1685.9
626.1 (32)[c]	n.o.[d]	623.7	n.o.	535.6	n.o.
580.5 (51)[e]	571.5 (0.015)	575.5	567.7	450.9	444.8
546.3 (1)[f]	n.o.	528.4	n.o.	471.2	n.o.
530.5 (73)[g]	514.6 (0.002)	527.5	512.0	404.9	n.o.

[a] Infrared intensity, km/mol. [b] Intensity, absorbance units after 12 K annealing. [c] Mostly in-plane Pt−H deformation. [d] Not observed. [e] Mostly in-plane C−H deformation. [f] Mostly Pt−C stretching mode. [g] Mostly out-of-plane C−H deformation.

K in solid argon. However, the softer neon matrix allows a 30% decrease in neon counterpart bands at 2010.4 and 571.5 cm^{-1} on photolysis and a 2-fold increase on annealing to 12 K. In addition two other important fundamentals are observed at 3317.5 and 2350.8 cm^{-1}.

The three highest bands are diagnostic bond-stretching fundamentals. The 3317.5 cm^{-1} band shifts 16.1 cm^{-1} with $^{13}C_2H_2$ and 739.7 cm^{-1} with C_2D_2. These shifts and appearance just above the σ_u C−H stretching mode of C_2H_2 characterize a

TABLE 7: Comparison of Calculated (BPW91) and Observed (Neon Matrix) Isotopic Frequencies (cm^{-1}) for Pt−η^2-(C_2H_2)

Pt(C_2H_2)		Pt($^{13}C_2H_2$)		Pt(C_2D_2)	
calc	obs	calc	obs	calc	obs
3269.4 (a_1, 3)[a]	n.o.[b]	3252.4	n.o.	2509.2	n.o.
3213.9 (b_2, 21)	3128.4 (0.0036)$_c$	3204.6	3119.3	2358.4	2339.1
1651.8 (a_1, 10)	1658.4 (0.0038)	1594.5	1599.0	1531.6	1571.2
858.0 (b_2, 76)	878.6 (0.0082)	849.6	869.5	692.6	724.4
651.9 (b_1, 71)	665.9 (0.0072)	649.0	663.1	506.2	500.5

[a] Mode symmetry, intensity km/mol. [b] Not observed. [c] Intensity, absorbance units, after 10 K annealing.

CC−H stretching mode. The 2350.8 cm^{-1} band shows no ^{13}C shift but shifts to 1685.9 cm^{-1} with C_2D_2 giving a 1.394 ratio. These observations and absorptions of PtH_2 at 2348.7 and 2365.7 cm^{-1} describe a Pt−H stretching mode.[27] The 2010.4 cm^{-1} band shifts 71.8 cm^{-1} with $^{13}C_2H_2$ and 113.4 cm^{-1} with C_2D_2, which characterizes a C≡C stretching mode coupled to C−H(D). Hence, we have described the HPtCCH molecule, and comparisons of calculated and observed isotopic frequencies (Table 6) confirm these assignments to HPtCCH. There is very good agreement in frequency positions and calculated isotopic shifts, remembering that anharmonicity in the C−H motion is not taken into account in the harmonic calculation. In addition the in-plane C−H deformation mode at 571.5 cm^{-1} is predicted at

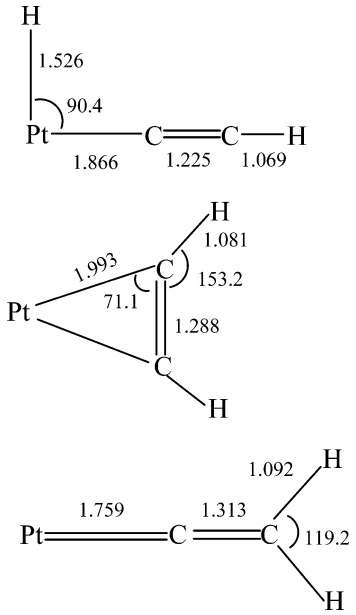

Figure 6. Converged structures (BPW91/6-311++G(d,p)/SDD) for Pt C_2H_2 isomers (lengths, angstroms; angles, degrees).

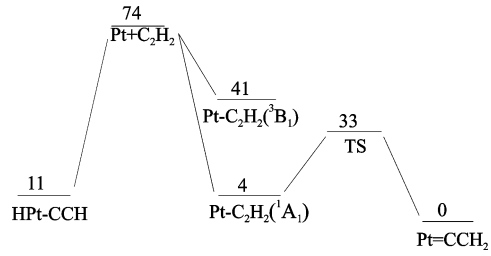

Figure 7. Energy profile diagram (BPW91/6-311++G(d,p)/SDD) for Pt C_2H_2 isomers (values in kcal/mol).

580.5 cm^{-1}, the out-of-plane C−H deformation predicted at 530.5 cm^{-1} is found at 514.6 cm^{-1}, and again the isotopic shifts match very well. The calculated intensities are qualitatively in agreement with the observed values. The lowest band at 514.6 cm^{-1} is weaker than predicted in part due to poor signal-to-noise in this region.

Pt−η^2-(C_2H_2). Group C bands at 1653.7, 882.8, and 666.2 cm^{-1} are attributed to the strong complex or metallacyclopropene, Pt−η^2-(C_2H_2). These bands are weak on deposition, increase on annealing, decrease on broad-band photolysis, but restore on further annealing. The 1653.7 cm^{-1} band shifts to 1598.5 cm^{-1} with $^{13}C_2H_2$ (1.0345 $^{12}C/^{13}C$ frequency ratio) and to 1550.9 cm^{-1} with C_2D_2 (1.0663 H/D frequency ratio), which are appropriate for the metallacyclopropene as observed for Ni−η^2-(C_2H_2) [18,47] and Pd−η^2-(C_2H_2).[26] With the mixed $^{12}C_2H_2$ + $^{13}C_2H_2$ sample two bands at 1653.7 and 1598.5 cm^{-1} are observed, suggesting a single C_2H_2 molecule and the Pt−η^2-(C_2H_2) complex assignment. The 882.8 and 666.2 cm^{-1} bands reveal isotopic shifts for deformation modes. The mixed C_2H_2, C_2HD, and C_2D_2 experiment gives a sharp matching triplet at 882.8, 867.6, and 731.1 cm^{-1}, which shows that a single acetylene molecule is involved here. An additional band observed at 3128.4 cm^{-1} in solid neon shifts 9.1 cm^{-1} with ^{13}C and 789.3 cm^{-1} with D, which is appropriate for a C−H stretching mode. Small, neon matrix shifts are observed for the above argon matrix bands.

Excellent agreement is found between the DFT calculations and observations for Pt−η^2-(C_2H_2). With the BPW91 functional the C−C stretching mode is predicted at 1651.8 cm^{-1}, which is 2−6 cm^{-1} below the matrix values. However an overestimation of 63.2 cm^{-1} is given by B3LYP for this mode. The predicted in-plane CCH deformation mode at 858.0 cm^{-1} (BPW91) and 877.7 cm^{-1} (B3LYP) and out-of-plane deformation at 651.9 cm^{-1} (BPW91) and 689.5 cm^{-1} (B3LYP) match experimental values very well. Table 7 compares calculated and observed neon matrix isotopic frequencies. The stronger C−H stretching mode is antisymmetric and the calculated (observed) shifts are 9.3 (9.1) cm^{-1} and 855.5 (789.3) cm^{-1} for ^{13}C and D; the effect of anharmonicity is again obvious in the C−H(D) stretching modes. The C−C stretching mode shifts are 57.3 (59.4) cm^{-1} and 120.2 (87.2) cm^{-1} for ^{13}C and D. The in-plane 8.4 (9.1) cm^{-1} and 165.4 (154.2) cm^{-1} and out-of-plane 2.9 (2.8) cm^{-1} and 145.7 (165.4) cm^{-1} deformation shifts, respectively, characterize these modes. Finally, the calculated infrared intensities are in qualitative agreement with the observed values although the C−C stretch is stronger than predicted, possibly due to underestimation of C−H, C−C stretching interaction by the calculation.

The weak 1618.3 cm^{-1} band in argon and split 1623.9, 1620.8 cm^{-1} bands in neon remain to be assigned. These bands behave like the above Pt−η^2-(C_2H_2) absorptions on annealing, photolysis, and isotopic substitution. These bands are probably due to Pt−η^2-(C_2H_2) perturbed by another species.

Pt−η^2-(C_2H_2)$_2$. A broad band with sharp shoulder at 1688.6 cm^{-1} observed on deposition grows on annealing to 30 K, but decreased on 240−290 nm photolysis and increased again on further annealing at the expense of Pt−η^2-(C_2H_2). This band is slightly higher than the C−C stretching mode in Pt−η^2-(C_2H_2) but still located in the C−C double bond stretching region. A smaller ^{13}C shift (47.7 cm^{-1}) and a larger deuterium shift (102.8 cm^{-1}) are observed for this band, which can be assigned to Pt−η^2-(C_2H_2)$_2$. The analogous molecule with two C_2H_2 ligands coordinated to the metal center was formed in the reaction of Pd with C_2H_2.[26]

DFT calculations support this assignment, and the results are summarized in Tables 3 and 4. The strongest absorption is the antisymmetric C−C stretching mode at 1708.0 cm^{-1} (BPW91) and 1767.9 cm^{-1} (B3LYP), respectively, which are in excellent agreement with the observed absorption. Again a slight overestimation is the systematic deviation.

Pt−CCH and Pt−CCH$^-$. Since CCH radical and CCH^- anion are abundant in the laser-ablated metal reactions[42] with C_2H_2, these intermediates may coordinate to metal atoms to form stable species. Sharp 1920.5 cm^{-1} and broader 1912.0 cm^{-1} absorptions are observed on deposition in solid argon: annealing and photolysis diminish the sharp in favor of the broader absorption. Neon matrix counterparts at 1924.4 and 1915.9 cm^{-1} favor the broader band more over the sharp absorption. These bands show the larger $^{12}C/^{13}C$ frequency ratio (1.0372) like HPtCCH in the triple bond region in contrast to Pt(C_2H_2) (1.0345) in the double bond region. Doublet distributions are observed in both mixed $^{12}C_2H_2$ + $^{13}C_2H_2$ and C_2H_4 + C_2HD + C_2D_2, experiments, which show that a single acetylene molecule is involved.

DFT calculations predict C−C stretching modes at 2037.1 cm^{-1} (BPW91) and 2099.9 cm^{-1} (B3LYP) for PtCCH, and at 1942.5 cm^{-1} (BPW91) and 2004.3 cm^{-1} (B3LYP) for Pt−CCH^-, and the anion modes are usually intense infrared absorbers. The sharp bands are assigned to the $PdCCH^-$ anion and the broader bands to $PdCCH^-$ aggregated with another molecule, presumably acetylene. We note that the calculated electron affinities for PdCCH (65.7 kcal/mol, BPW91 and 61.9 kcal/mol, B3LYP) are near the 66.9 kcal/mol experimental value for CCH.[47]

Reaction Mechanisms and Comparison with Surface Chemistry. The initial bonding of Pt atom to C_2H_2 adopts two different modes: side-on to the C−C triple bond forming a strong π-type complex, Pd−η^2-(C_2H_2) (reaction 1), or interaction with the C−H bond forming the insertion product, HPtCCH (reaction 2). (The given energy differences are from BPW91 calculations.)

$$\mathrm{Pt}\ (^3D_3) + \mathrm{C_2H_2}\ (^1\Sigma_g^+) \rightarrow [\mathrm{Pt}-\eta^2\text{-}(\mathrm{C_2H_2})\ (^3B_1)] \rightarrow \mathrm{Pt}-\eta^2\text{-}(\mathrm{C_2H_2})\ (^1A_1) \quad \Delta E = -70.5\ \mathrm{kcal/mol} \quad (1)$$

$$\mathrm{Pt}\ (^3D_3) + \mathrm{C_2H_2}\ (^1\Sigma_g^+) \rightarrow \mathrm{HPt-CCH}\ (^1A') \quad \Delta E = -63.4\ \mathrm{kcal/mol} \quad (2)$$

Laser ablation produces ground-state $^3D_3$ Pt atom as well as excited singlet states; however, collisions with argon atoms during deposition relaxes most of excited Pt atoms. Reaction 1 most likely first forms the triplet intermediate, Pt−η^2-(C_2H_2) ($^3B_1$), which is 33.6 kcal/mol exothermic. Then the $^3B_1$ state is relaxed by the cold argon matrix to the 36.9 kcal/mol lower energy $^1A_1$ ground state. If Pt atom directly encounters the C−H bond instead of the C−C bond, the insertion reaction is spontaneous on the basis of the growth of HPt−CCH absorptions on annealing to 25−30 K in solid argon. In this reaction spin−orbit coupling plays an important role, and triplet Pt crosses the mixed region of the triplet−singlet potential energy curve. Recall the reactions of thermal and laser-ablated Pt atoms with H_2 in low-temperature matrixes, where ground-state Pt reacts with H_2 spontaneously to form the insertion product, PtH_2, in the $^1A_1$ state.[27]

Adsorption and dehydrogenation of acetylene on the Pt(111) surface have been investigated extensively.[1−6] The thermally induced rearrangements and reactions of acetylene on the Pt surface produce first vinylidene (Pt_x−CCH_2) and then ethylidyne (Pt_x−CCH_3), suggesting a disproportionation reaction of acetylene to ethynyl (Pt_x−CCH) also occurs. Here a hydrogen-poor ethynyl simultaneously formed on the surface provides a hydrogen atom to produce ethylidyne. As observed in the low-temperature matrix, the spontaneously formed insertion product HPtCCH is the first step in generating a hydrogen atom in this process. During the surface annealing, the weak Pt−H bond is broken and the hydrogen atom migrates to adsorbed vinylidene to form ethylidyne (Pt_x−CCH_3).

The most interesting reaction product observed in this system is Pt═CCH_2, which is the lowest energy on the Pt−C_2H_2 potential energy surface. Upon 240−290 nm photolysis Pt−η^2-(C_2H_2) rearranges directly by 1,2-hydrogen migration to form Pt═CCH_2, which is observed after deposition and increased on ultraviolet photolysis (Figure 1) in solid argon. This rearrangement also occurs in the softer neon matrix on annealing to 10−12 K as absorptions for both products increase. Apparently reaction 1 is sufficiently exothermic to activate the rearrangement in reaction 3.

$$\mathrm{Pt}-\eta^2\text{-}(\mathrm{C_2H_2}) \xrightarrow{240-290\ \mathrm{nm}} \mathrm{Pt{=}CCH_2} \quad (3)$$

We find no evidence for 1,3-rearrangement from HPtCCH to Pt═CCH_2 because the absorptions of HPtCCH increase on annealing and photolysis. In transition metal complex chemistry the hydrido metal intermediate (L_nMH−CCH) might convert to the corresponding vinylidene through 1,3-rearragement. However, theoretical calculations indicate that 1,3-rearrangement has a higher activation energy barrier than direct 1,2-rearragement.[13] Wakatsuki et al. found that formation of the vinylidene complex from the hydrido intermediate should occur via an intermolecular process rather than an intramolecular 1,3-rearrangement, which is much higher in energy.

In contrast to the Pd/C_2H_2 system where Pd_2−η^2-C_2H_2 was observed as a secondary reaction product,[28] no evidence was found here for analogous diplatinum species computed in complex and vinylidene isomeric forms to assist in their identification. This is probably due to a large energy barrier for reaction of Pt (^3D) + Pt−η^2-(C_2H_2) ($^1A_1$) because of forbidden symmetry. However, reactions of Pd (^1S) + Pd−η^2-(C_2H_2) ($^1A_1$) gave Pd_2−η^2-(C_2H_2) ($^1A_1$) with a very low energy barrier; although the reaction of Pt_2 with C_2H_2 is feasible on the basis of theoretical calculations and surface studies,[1,2] this reaction is not observed here because very little Pt_2 dimer was generated in our experiment (the Pt_2 absorptions in the IR are electronic transitions[44]).

The vinylidene species is also observed on the Pt(111) surface on annealing to 125 K during acetylene thermal rearrangement, which is stabilized to μ-vinylidene on much higher temperature annealing (>300 K).[4−6] However, in solid argon the vinylidene species is not produced by thermal annealing (25−40 K), even though Pt═CCH_2 is lower in energy, but ultraviolet photolysis does affect the rearrangement. By contrast, on annealing solid neon to 10−12 K allowing reagent diffusion, some of the reaction proceeds through Pt−η^2-(C_2H_2) to Pt═CCH_2.

Bonding in M−η^2-(C_2H_2) and M═CCH_2 (M = Ni, Pd, Pt). The C═C stretching frequencies for M−η^2-(C_2H_2) complexes are observed at 1634.8 cm^{-1} (Ni),[18,47] 1709.6 cm^{-1} (Pd),[26] and 1653.7 cm^{-1} (Pt), showing a difference in interaction between the metal atoms and acetylene. This difference is also revealed in the C−H deformation frequencies as well: 843.2, 655.0 cm^{-1} (Ni), 765.8, 674.5 cm^{-1} (Pd), and 882.8, 662.2 cm^{-1} (Pt), where the reference for C_2H_2 in solid argon is 736.9 cm^{-1}.[49] On the basis of the DFT calculation, the C═C bond length in Pt−η^2-(C_2H_2) is 1.288 Å and the Ni complex is the same (BPW91), but this bond is 0.02 Å shorter in Pd−η^2-(C_2H_2). Furthermore the distances from metal to carbon are shorter for Ni and Pt than Pd. These pieces of evidence suggest stronger interactions between Ni, Pt, and C_2H_2 than between Pd and C_2H_2. The calculation of the CC bond gives 1.209 Å for C_2H_2. The binding energies in the M−η^2-(C_2H_2) complexes are calculated to be 41 kcal/mol (Ni), 40 kcal/mol (Pd), and 70 kcal/mol (Pt), showing the very strong Pt−C_2H_2 bond.

For the metal−vinylidene complexes Pt═CCH_2 shows some unique properties: a very short Pt−C double bond (116 kcal/mol) and global minimum energy structure in contrast to Ni[47] and Pd,[26] and Pt withdraws charge (−0.06) from CCH_2 in contrast to Pd (+0.10) and Ni (+0.20), which donate charge to CCH_2. In the valence approximation the main contribution to double bonding is from the σ bond of $6s^1$ (Pt) and sp hybridized orbital (:CCH_2) and the π bond of $d_\pi{}^1$ (Pt) and p^1 (:CCH_2), which gives an energetically stabilized vinylidene. However, for palladium the ground state is $5s^04d^{10}$, which favors the π-type complex instead of the vinylidene complex.

Conclusion

Platinum atoms react with acetylene on condensation in excess argon and neon to form the vinylidene Pt═CCH_2, a strong π-type complex Pt−η^2-(C_2H_2), and the insertion product HPtCCH, which are identified by $^{13}C_2H_2$, C_2D_2, and C_2HD isotopic substitution on the observed fundamental frequencies. DFT calculations (BPW91 and B3LYP functionals) are performed to optimize the stable structures and produce the isotopic vibrational frequencies. The $PtCCH_2$ vinylidene, which is the

global minimum on the potential energy surface, absorbs at 3022.8 cm^{-1} (C−H stretching), 1716.5 cm^{-1} (C−C stretching), and 707.9 cm^{-1} (CH_2 deformation) in the argon matrix. The HPtCCH molecule is characterized by a C−C stretching mode at 2016.2 cm^{-1}. DFT calculations give a 90° H−Pt−C bond angle for HPtCCH, which is sd hybridized at Pt, and 9−10 kcal/mol higher energy. The absorptions of the Pt−η^2-(C_2H_2) complex, which is 3−4 kcal/mol higher in energy than $PtCCH_2$, are observed at 1653.7, 882.8, and 666.2 cm^{-1}. The Pt−η^2-$(C_2H_2)_2$ complex is identified by C−C stretching at 1688.6 cm^{-1}. Finally the $PtCCH^-$ anion is also assigned in this study.

The initial bonding of Pt atom to C_2H_2 adopts two different modes: side-on to C−C triple bond, involving π-interactions and forming the metallacyclopropene Pd−η^2-(C_2H_2), or interaction with the C−H bond, forming the insertion product, HPtCCH. The Pt atom insertion reaction with C_2H_2 is spontaneous on the basis of the growth of absorption of HPt−CCH on annealing to 10−12 K in solid neon or to 25−30 K in solid argon. In this reaction spin−orbit coupling plays an important role and triplet Pt crosses the mixed region of the triplet−singlet potential energy surface. Upon 240−290 nm photolysis P−η^2-(C_2H_2) rearranges directly by 1,2-hydrogen migration to form Pt═CCH_2. This rearrangement also occurs on annealing to 12 K in solid neon as both product absorptions increase: the formation of Pt−η^2-(C_2H_2) is sufficiently exothermic to activate rearrangement to the more stable Pt═CCH_2 form.

Acknowledgment. We gratefully acknowledge support for this work from N.S.F. Grant CHE 00-78836.

References and Notes

(1) Megiris, C. E.; Berlowitz, P.; Butt, J. B.; Kung, H. H. *Surf. Sci*. **1985**, *159*, 184.
(2) Rashidi, M.; Puddephatt, R. J. *J. Am. Chem. Soc*. **1986**, *108*, 7111.
(3) Abon, M.; Billy, J.; Bertolini, J. C. *Surf. Sci.* **1986**, *171*, L387.
(4) Avery, N. R. *Langmuir* **1988**, *4*, 445.
(5) Cremer, P. S.; Su, X. C.; Shen, Y. R.; Somorjai, G. A. *J. Phys. Chem. B* **1997**, *101*, 6474.
(6) Kose, R.; Brown, W. A.; King, D. A. *J. Am. Chem. Soc*. **1999**, *121*, 4845.
(7) Azad, S.; Kaltchev, M.; Stacchiola, D.; Wee, G.; Tysoe, W. T. *J. Phys. Chem. B* **2000**, *104*, 3107, and references therein. See also the early work of: Gates, J. A.; Kesmodel, L. L. *J. Chem. Phys.* **1982**, *76*, 4281. Gates, J. A.; Kesmodel, L. L. *Surf. Sci.* **1983**, *123*, 68.
(8) (a) Gallo, M. M.; Hamilton, T. P.; Schaefer, H. F., III. *J. Am. Chem. Soc.* **1990**, *112*, 8714. (b) Jensen, J. H.; Morokuma, K.; Gordon, M. S. *J. Chem. Phys.* **1994**, *100*, 1981.
(9) (a) Chen, W.-C.; Yu, C.-H. *Chem. Phys. Lett.* **1997**, *227*, 245. (b) Hayes, R. L.; Fattal, E.; Govind, N.; Carter, E. A. *J. Am. Chem. Soc.* **2001**, *123*, 641.
(10) (a) Chen, Y.; Jonas, D. M.; Kinsey, J. L.; Field, R. W. *J. Chem. Phys.* **1989**, *91*, 3976. (b) Ervin, K. M.; Ho, J.; Lineberger, W. C. *J. Chem. Phys.* **1989**, *91*, 5974.
(11) (a) Bruce, M. I. *Chem. Rev.* **1991**, *91*, 197. (b) Werner, H. *Angew. Chem.* **1990**, *102*, 1109; *Angew. Chem., Int. Ed. Engl.* **1990**, *29*, 1077.
(12) Stegmann, R.; Frenking, G. *Organometallics* **1998**, *17*, 2089.
(13) Wakatsuki, Y.; Koga, N.; Werner, H.; Morokuma, K. *J. Am. Chem. Soc.* **1997**, *119*, 360, and references therein.
(14) Glendening, E. D.; Strang, M. L. *J. Phys. Chem. A*, in press.
(15) Ozin, G. A.; McIntosh, D. F.; Power, W. J.; Messmer, R. P. *Inorg. Chem.* **1981**, *20*, 1782.
(16) Kasai, P. H. *J. Am. Chem. Soc.* **1982**, *104*, 1165.
(17) Kasai, P. H. *J. Am. Chem. Soc*. **1983**, *105*, 6704.
(18) Kline, E. S.; Kafafi, Z. H.; Hauge, R. H.; Margrave, J. L. *J. Am. Chem. Soc.* **1987**, *109*, 2402.
(19) (a) Burkholder, T. R.; Andrews, L. *Inorg. Chem.* **1993**, *32*, 2491 (Al, Ga, In + C_2H_2). (b) Chertihin, G. V.; Andrews, L.; Taylor, P. R. *J. Am. Chem. Soc.* **1994**, *116*, 3513 (Al + C_2H_2).
(20) Manceron, L.; Andrews, L. *J. Am. Chem. Soc*. **1985**, *107*, 563.
(21) (a) Martin, J. M. L.; Taylor, P. R.; Hassanzadeh, P.; Andrews, L. *J. Am. Chem. Soc.* **1993**, *115*, 2510. (b) Andrews, L.; Hassanzadeh, P.; Martin, J. M. L.; Taylor, P. R. *J. Phys. Chem.* **1993**, *97*, 5839 (B + C_2H_2).
(22) Thompson, C. A.; Andrews, L. *J. Am. Chem. Soc*. **1996**, *118*, 10242 (Be, Mg + C_2H_2).
(23) Kline, E. S.; Kafafi, Z. H.; Hauge, R. H.; Margrave, J. L. *J. Am. Chem. Soc*. **1985**, *107*, 7559.
(24) Chenier, J. H. B.; Howard, J. A.; Mile, B.; Sutcliffe, R. *J. Am. Chem. Soc*. **1983**, *105*, 788.
(25) Kasai, P. H. *J. Phys. Chem*. **1982**, *86*, 4092, *J. Am. Chem. Soc.* **1992**, *114*, 3299.
(26) Wang, X.; Andrews, L. *J. Phys. Chem. A* **2003**, *107*, 337 (Pd + C_2H_2).
(27) Andrews, L.; Wang, X.; Manceron, L. *J. Chem. Phys*. **2001**, *114*, 1559 (Pt + H_2).
(28) Andrews, L.; Wang, X.; Alikhani, M. E.; Manceron, L. *J. Phys. Chem. A* **2001**, *105*, 3052 (Pd + H_2).
(29) Wang, X.; Andrews, L. *J. Am. Chem. Soc*. **2002**, *124*, 5636 (W + H_2).
(30) Wang, X.; Andrews, L. *J. Am. Chem. Soc*. **2001**, *123*, 12899 (Au + H_2).
(31) Wang, X.; Andrews, L. *J. Phys. Chem. A* **2002**, *106*, 3706 (Rh + H_2)
(32) Bare, W. D.; Citra, A.; Chertihin, G. V.; Andrews, L. *J. Phys. Chem. A* **1999**, *103*, 5456.
(33) Wang, X.; Andrews, L. *J. Phys. Chem. A* **2001**, *105*, 5812.
(34) Frisch, M. J.; Trucks, G. W.; Schlegel, H. B.; Scuseria, G. E.; Robb, M. A.; Cheeseman, J. R.; Zakrzewski, V. G.; Montgomery, J. A., Jr.; Stratmann, R. E.; Burant, J. C.; Dapprich, S.; Millam, J. M.; Daniels, A. D.; Kudin, K. N.; Strain, M. C.; Farkas, O.; Tomasi, J.; Barone, V.; Cossi, M.; Cammi, R.; Mennucci, B.; Pomelli, C.; Adamo, C.; Clifford, S.; Ochterski, J.; Petersson, G. A.; Ayala, P. Y.; Cui, Q.; Morokuma, K.; Malick, D. K.; Rabuck, A. D.; Raghavachari, K.; Foresman, J. B.; Cioslowski, J.; Ortiz, J. V.; Stefanov, B. B.; Liu, G.; Liashenko, A.; Piskorz, P.; Komaromi, I.; Gomperts, R.; Martin, R. L.; Fox, D. J.; Keith, T.; Al-Laham, M. A.; Peng, C. Y.; Nanayakkara, A.; Gonzalez, C.; Challacombe, M.; Gill, P. M. W.; Johnson, B.; Chen, W.; Wong, M. W.; Andres, J. L.; Gonzalez, C.; Head-Gordon, M.; Replogle, E. S.; Pople, J. A. *Gaussian 98*, revision A.6; Gaussian, Inc.: Pittsburgh, PA, 1998.
(35) (a) Becke, A. D. *J. Chem. Phys.* **1993**, *98*, 5648. (b) Lee, C.; Yang, W.; Parr, R. G. *Phys. Rev. B* **1988**, *37*, 785.
(36) (a) Becke, A. D. *Phys. Rev. A* **1988**, *38*, 3098. (b) Perdew, J. P.; Wang, Y. *Phys. Rev. B* **1992**, *45*, 13244.
(37) (a) Krishnan, R.; Binkley, J. S.; Seeger, R.; Pople, J. A. *J. Chem. Phys.* **1980**, *72*, 650. (b) Frisch, M. J.; Pople, J. A.; Binkley, J. S. *J. Chem. Phys.* **1984**, *80*, 3265.
(38) Andrae, D.; Haussermann, U.; Dolg, M.; Stoll, H.; Preuss, H. *Theor. Chim. Acta* **1990**, *77*, 123.
(39) Jacox, M. E.; Olson, W. B.; *J. Chem. Phys*. **1987**, *86*, 3141.
(40) Jacox, M. E.; *J. Phys. Chem. Ref. Data* **1994**, *3*, 32, and references therein.
(41) Forney, D.; Jacox, M. E.; Thompson, W. E. *J. Mol. Spectrosc*. **1995**, *170*, 178.
(42) Andrews, L.; Kushto, G. P.; Zhou, M.; Willson, S. P.; Souter, P. F. *J. Chem. Phys*. **1999**, *110*, 4457.
(43) Wang, X.; Andrews, L. *J. Phys. Chem. A* **2001**, *105*, 7799.
(44) Li, S.; Weimer, H. A.; VanZee, R. J.; Weltner, W., Jr. *J. Chem. Phys.* **1997**, *106*, 2583.
(45) Herzberg, G. *Infrared and Raman Spectra of Polyatomic Molecules*; Van Nostrand: New York, 1945.
(46) Jacox, M. E. *Chem. Phys.* **1994**, *189*, 149.
(47) Similar laser-ablation experiments with Ni and DFT calculations confirm the C═C stretching and C−H deformation assignments of the Rice group[18] to Ni−η^2-(C_2H_2) but the bands assigned to $NiCCH_2$ are most likely due to Ni−η^2-(C_2H_2) in a different matrix site.
(48) Ervin, K. M.; Lineberger, W. C. *J. Chem. Phys.* **1991**, *95*, 1167.
(49) Andrews, L.; Johnson, G. L.; Kelsall, B. J. *J. Phys. Chem.* **1982**, *86*, 3374.
(50) Reed, A. E.; Curtiss, L. A.; Weinhold, F. *Chem. Rev.* **1988**, *88*, 899.